[UCI]I804:24011-200000266529

2018년 2월 석사학위논문 Surface Characteristics of Zinc Coatings on the PEO-treated Ti-6Al-4V by RF-sputtering 황 인 조

2018년 2월
석사학위논문

Surface Characteristics of Zinc Coatings on the PEO-treated Ti-6Al-4V by RF-sputtering

조선대학교 대학원

광기술공학과

황 인 조

Surface Characteristics of Zinc Coatings on the PEO-treated Ti-6Al-4V by RF-sputtering

RF-sputtering법으로 PEO 처리된 Ti-6Al-4V 합금
표면에서 아연코팅 피막의 표면특성

2018년 2월 23일

조선대학교 대학원

광기술공학과

황 인 조

Surface Characteristics of Zinc Coatings on the PEO-treated Ti-6Al-4V by RF-sputtering

지도교수 최 한 철

이 논문을 공학 석사학위신청 논문으로 제출함

2017년 10월

조선대학교 대학원

광기술공학과

황 인 조

황인조의 석사학위논문을 인준함

위원장 조선대학교 교수 손 미 경 (인)

위 원 조선대학교 교수 안 상 건 (인)

위 원 조선대학교 교수 최 한 철 (인)

2017년 11월

조선대학교 대학원

CONTENTS

LIST OF TABLES

LIST OF FIGURES

국 문 초 록

RF-sputtering법으로 PEO 처리된 Ti-6Al-4V 합금 표면에서 아연코팅 피막의 표면특성

황 인 조
지도교수 : 최 한 철, 공학/치의학 박사
광기술공학과
조선대학교 대학원

티타늄 (CP-Ti) 및 티타늄 합금 (Ti-6Al-4V)은 생체적합성, 부식저항성, 기계적 특성이 우수하기 때문에 정형외과의 본 플레이트와 인공관절 등 임플란트 재료뿐만 아니라 치과용 임플란트 재료로 널리 사용되고 있다. 그러나 Ti 금속은 생체불활성 재료로 골 융합을 직접적으로 유도하지 않기 때문에 충분한 골 융합이 이루어지기까지 상당한 시간이 필요하다. 이 때문에 임플란트 표면을 개선하기 위해 많은 연구를 하고 있다. 이 들 연구 중에서도, 인산칼슘 (Ca/P)은 주변 뼈 조직에 강한 친화성과 뼈 형성을 유도하는 능력이 우수하여 Ti 합금 임플란트에 코팅 재료로 적용되고 있다. 뼈의 무기성분으로 Sr, Mg, Zn, 및 Si 과 같은 원소들은 뼈 형성에 중요한 역할을 하고, 또한 결정화 및 기계적 성질과 같은 뼈 특성에 영향을 미친다. 따라서 본 연구에서는 플라즈마 전해 산화법을 이용하여 티타늄 합금에 마이크로 포아를 형성한 후, 거칠기를 부여한 표면에 물리적인 증착법을 이용하여 아연 (Zn)을 코팅함으로써 뼈와의 접착성을 극대화시키는 연구를 진행하였다. 코팅공정은 두 단계로 실시하였다; 1) 표면에 마이크로 포아를 형성함과 동시에 수산화인회석의 코팅막의 결합력을 증진시키기 위해 0.15 M $Ca(OAc)_2$ + 0.02 M CGP 를 280 V에서 3분 간 DC power supply를 이용하여 인가하였다. 2) 마이크로 포아를 형성 한 표면에 RF-magnetron sputtering법을 이용하여 아연 (Zn)을 1, 및 3분 간 코팅하였다. 두 단계로 처리된 Ti-6Al-4V 합금의 표면특성은 주사전자현미경, EDS, 및 X-선 회절분석을 사용하여 분석하였다. MC3T3세포를 사용하여 생물학적 변화가 다른 조건에 미치는 영

향을 조사하였다. 이러한 실험을 통하여 다음과 같은 결론을 얻었다.

1. Ti-6Al-4V에서 PEO 처리 후 양극산화층을 분석한 결과, 균일하고 많은 마이크로 포어가 배열된 양상을 보였으며, 물리적인 방법으로 Zn를 코팅한 경우에는 마이크로 포어 내부와 표면에 더 많은 원형의 코팅물질 입자들이 관찰되었다.
2. 스퍼터링 시간이 길어짐에 따라 TiO_2의 결정구조는 비정질상이 증가하고 결정상이 감소하였다.
3. MC3T3-E1 세포 실험 결과, 세포 성장은 PEO 포아 표면만 존재하는 경우 보다는 마이크로 포어 표면에 아연 코팅한 경우가 더 우수하였다. 세포 생존력은 1분 동안 Zn 코팅한 경우가 세포의 성장과 생존력이 가장 우수하였다.

결론적으로, PEO 처리 후, RF 스퍼터링으로 아연코팅 처리한 Ti-6Al-4V 합금은 마이크로의 표면에 세포가 잘 자랄 수 있는 환경을 제공하였으며, 골과 임플란트 계면에서 골 유착을 향상시키는 우수한 환경을 제공할 것으로 생각된다.

Ⅰ. INTRODUCTION

Titanium (Ti) is known to be one of the valve metals (Al, Ta, Nb, V, W) whose Ti oxide (mainly TiO_2) is continuously formed on its surface when exposed to an atmosphere containing oxygen, and surface corrosion is suppressed by this layer. In this case, the generated natural oxide film has a thickness of 2 to 5 nm and improves the corrosion resistance of the metal. Such as metal corrosion resistance increases the biocompatibility by inhibiting dissolution of metal in vivo[1]. However, the degree of osseointegration between the naturally occurring Ti oxide layer and the bone is weak and it is continuously destroyed after implantation. Orthopedic implants made of titanium have a life expectancy of 10 to 15 years[2,3]. For this reason, many studies have been actively conducted to improve the bioactivity through the Ti surface modification in order to improve the bonding of the implants in the bone tissue and the bone. In the natural bone, bone is mainly composed of Ca and P, additionally, and contained the mineral elements such as Si, Sr, Mn, Mg, and Zn and so on. Calcium (Ca) activates Ca-sensing receptors in osteoblast cells. Phosphate (P) shows anti-inflammatory effect and stimulates bone formation in vitro by activation protein synthesis in osteoblasts. Silicon (Si) shows essential for metabolic processes, formation and calcification of bone tissue. Strontium (Sr) shows beneficial effects on bone cells and bone formation in vivo. Manganeses (Mn) is known to have beneficial role for the skeleton and mineralization[4]. Magnesium (Mg) is known to have increased bone cell adhesion and stability. Especially, zinc (Zn) is found in numerous enzymes and is known as a trace elements in vertebrates. The Zn ion can affect the body and the skeleton in particular. It has been demonstrated to have a wide variety if roles in various processes in the mammalian system, such as immune defense and wound healing[5].

To enhanced biocompatibility, surface treatment of Ti alloys were widely used for biomaterial such as pulsed laser deposition, plasma spray, magnetron sputtering, alkali treatment, electron-beam physical vapor deposition, and electrochemical deposition[6-11]. Especially, Plasma electrolytic oxidation is known as an excellent method in the biocompatibility of biomaterial due to quickly coating time and controlled coating condition[12]. The plasma electrolytic oxidation oxide layer and diameter modulation of Ti alloys can be obtained function of improvement of cell adhesion[13].

Also, radio frequency (RF) magnetron sputtering is a versatile deposition technique that can produce uniform, dense and hard coatings with a thickness < 1 mm that are homogeneous in structure and composition[14]. Even though electro-deposited and RF-sputtered surface have many advantages, comparison of surface characteristics between electro-deposited and RF-sputtered surface was not researched. Zn coated micro-pore surface can improve bone strength, reduce interfacial failure[15]. According to a previous study, Ti-6Al-4V after plasma electrolytic oxidation in solutions containing Ca, P, and Zn ions presented superior in improving the biocompatibility if the human body[12,16]. And, studies have been presented that enhanced the calcification of osteoblasts when Zn is combined to biological coating materials by sputtering method[17].

Therefore, in the study, we investigated surface characteristics of zinc coatings on the PEO-treated Ti-6Al-4V by RF-sputtering.

Ⅱ. BACKGROUND

2.1. Properties of bio-metallic materials

Orthopedic and dental implants, which are implanted in human tissues for long periods of time, must not be toxic to living cells and have a long lifespan because the fatigue load is applied for a long time. In addition, the abrasion resistance between the femoral head and the acetabular cup should be excellent[18]. Generally, metallic materials for living body which should have such characteristics include stainless steel (316L), cobalt (Co-Cr) alloys, titanium and alloys. 316L is used as a medical material because of its low cost and good corrosion resistance, but it cannot withstand continuous load and it can cause side effects that weaken bone strength. Titanium and Ti-6Al-4V alloys, on the other hand, have excellent biocompatibility with bone-like elastic modulus and have been widely used as artificial joints and dental implant materials[19,20]. Table 1 shows the properties of biomaterials when selecting or developing bio alloys.

The affinity of the bio alloys is determined by the reactivity between the initial bone fiber cell and the metal and the reactivity with the metal ion or metal oxide eluted in the body, that is, the corrosion product with the bone fiber cell, the biological fluid, the blood. Ti, Nb, and Zr are known as metal elements that are excellent in corrosion resistance in vivo, and are not toxic to corrosion products, fibrous cells, biological fluids, and the like and thus have excellent biocompatibility. Fig. 1 shows that the elements of Fe, Co, Bi, Ag, Sr, Mg, V, Cu, Zn, Cd and Hg are highly cytotoxic[21]. On the other hand, Ti, Ti alloys, Ta, Nb, Zr, and Pt are elements or alloys with excellent biocompatibility[20,21].

Table 1. Properties of biomaterial[20]

Biocompatibility	- Osseointegration - Bio-corrosion resistance - Adverse tissue reaction
Mechanical properties	- Elastic modulus - Tensile, yield strength - Elongation - Toughness - Fatigue crack initiation, and propagation - Hardness, wear resistance

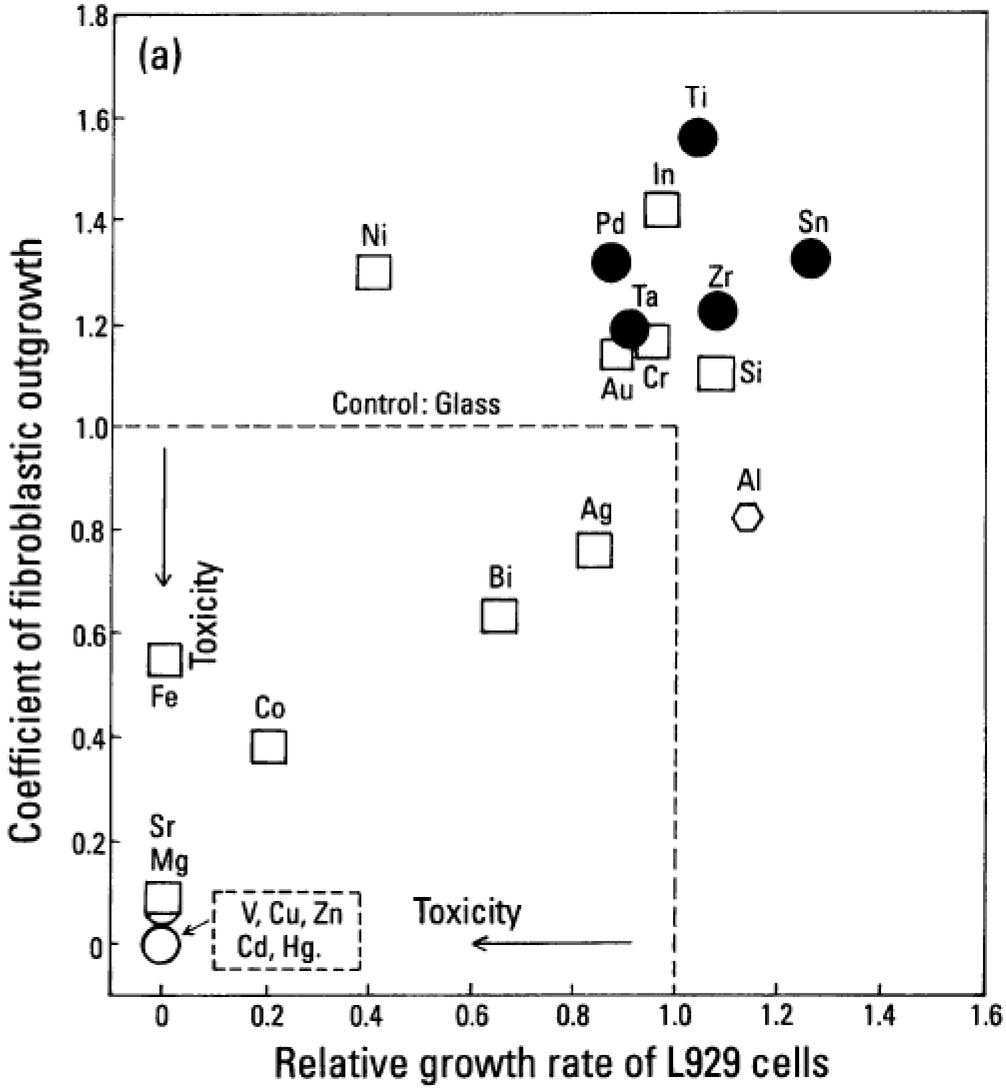

Fig. 1. Cytotoxicity of pure metals[21].

2.2. Ti alloy as biomaterial

The metallic materials used as biomaterials must take into account the biostability associated with the immune response and the biocompatibility associated with the properties of the material. Due to these demanding requirements, metal materials that can be used as biomaterials are extremely limited; stainless steel (316L), Co-Cr alloys, Ti and Ti-6Al-4V alloy, etc. Among them, the Ti alloy has very low density, the elastic modulus most similar to that of the bone tissue, and has excellent mechanical and corrosion resistance characteristics, and is most popular as an implant material.

Pure Ti is an element belonging to 4 period 4 tribes on the periodic table and divided into 4 types from grade Ⅰ to Ⅳ, representatively, it is distinguished as Ti-6Al-4V and Ti-6Al-4V extra low interstitial (ELI). Ti is the ninth most abundant element following O, Si, Al, Fe, Ca, Na, K, and Mg among the constituents of the crust, Table 2 shows the composition of Ti and its alloys[23]. Ti has a specific gravity of 4.54 g/cm^3 and is 1.6 times heavier than Al (2.71 g/cm^3) and 60 % lighter than Fe (7.87 g/cm^3), It corresponds to light metal. Pure Ti has a melting point of 1668 ℃ and higher than Fe (1536 ℃), and has a low coefficient of thermal expansion and thermal conductivity[24,25].

As shown in Fig. 2, the Ti-6Al-4V alloys consists of two alloys, HCP (α phase) and BCC (β phase), the α phase is stable from room temperature to 882.5 ℃ and β phase is stable at temperatures above 882.5 ℃. The usual Ti-6Al-4V alloy is manufactured by heating the β phase transformation temperature as closely as 882.5 ℃, in order to precipitate β phase particles on a fine α phase base structure and grain boundary, was annealing. Phase transition from α phase to β phase occur at a temperature of 882.5 ℃ due to its high melting point, thermal conductivity and electric conductivity[26,27]. Table 3 shows the physical property of Ti with phase transformation at 882.5 ℃[28].

Ti is excellent in corrosion resistance and firmly adhering to the titanium oxide film formed on the surface, so that it has a large effect of inhibiting corrosion into the inside of the material, and is immediately regenerated even if the passivation film is destroyed.

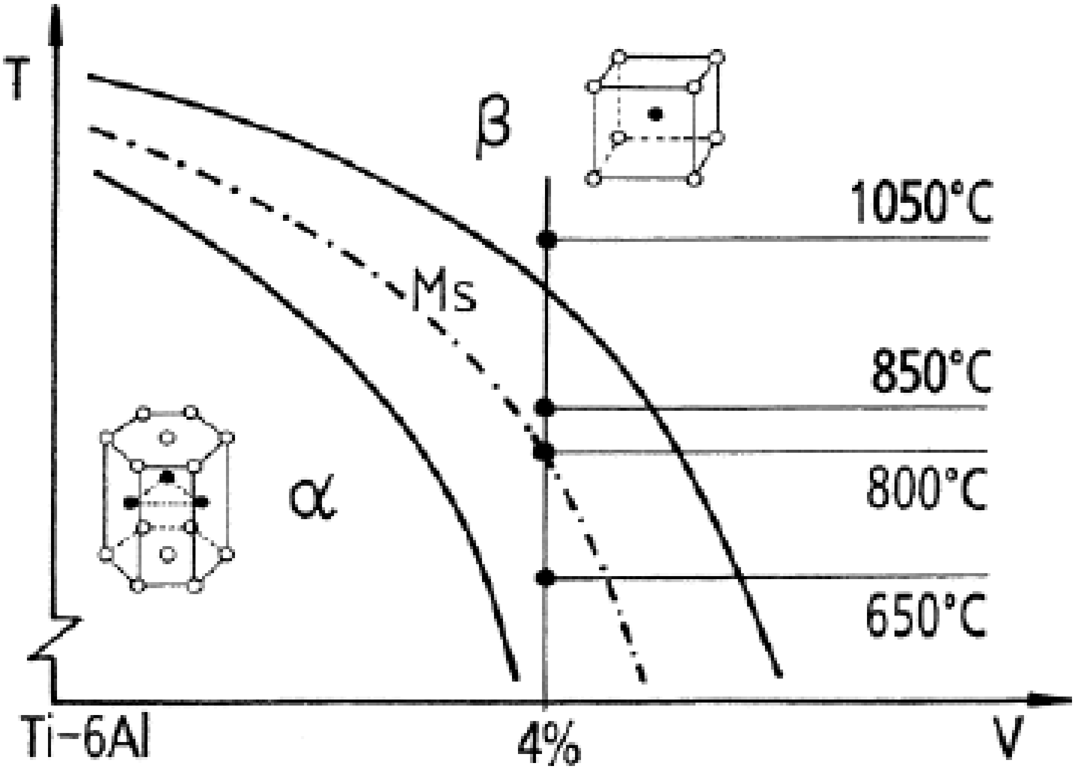

Fig. 2. Allotropic transformation of titanium[26,27].

Table 2. Composition of CP titanium and alloys (wt. %)[23)]

Titanium	N	C	H	Fe	O	Al	V	Ti
CP grade I	0.03	0.10	0.015	0.02	0.18	-	-	balance
CP grade II	0.03	0.10	0.015	0.03	0.25	-	-	balance
CP grade III	0.03	0.10	0.015	0.03	0.35	-	-	balance
CP grade IV	0.03	0.10	0.015	0.05	0.40	-	-	balance
Ti-6Al-4V alloy	0.05	0.08	0.015	0.30	0.20	5.50-6.75	3.50-4.50	balance
Ti-6Al-4V ELI alloy	0.05	0.08	0.012	0.10	0.13	5.50-6.50	3.50-4.50	balance

Table 3. Physical property of titanium[28)]

Property	α-Ti (> 99.9 wt. %)
Linear expansion coefficient	$8.36 \cdot 10^{-6}$ K
Thermal conductivity	14.99 W/m · K
Specific heat capacity	523 J/kg · K
Electrical resistivity	$5.6 \cdot 10^{-7}$ Ω · m
β / α Transform. temperature	882.5 ℃
Young's modulus	115 GPa
Shear modulus	44 GPa
Poisson's ratio	0.33
Density	4.51 g/cm^3

2.3. Titanium dioxide (TiO_2)

In general, metals are exposed to the atmosphere and form an oxide film naturally. This is caused by a reaction with gas in the atmosphere. Theoretically, Ti forms oxides such as TiO, TiO_2, Ti_2O_3 and Ti_3O_5, and TiO_2 is the most stable oxide[29]. When the Ti implant is placed in the human body, the surrounding tissue of the implant surface is connected to the TiO_2 layer. Ti surfaces can bond tightly to bone tissue directly by forming apatite layers between the interface. This bone-like apatite layer can accelerate the process of osseointegration[30]. When this oxide is exposed to oxygen, an oxide film having a thickness of 10 Å is formed within 1/1000 second, and within one minute, this oxide film becomes 100 Å thick. The biocompatibility of the Ti implants is determined by the surface characteristics of the TiO_2 layer, when oxygen is sufficiently supplied, the formed TiO_2 has a high bioactivity on the electrically negatively charged surface, and hydroxyl groups (OH^-) are well formed on the surface. In addition, it can be said that the implant is passivated that if the implant is oxidized and the oxide film is not destroyed under physiological conditions. These passivated Ti are very few[31].

In addition, TiO_2 is the only naturally occurring oxide of Ti at atmospheric pressure, exhibits three polymorphs; anatase, rutile, and brookite. It is classified according to the amorphous state and the temperature change, and be transferred from a metastable brookite and an anatase phase to a stable rutile phase[32]. Brookite phase is a relatively unstable substance as orthorhombic structure and exists mainly in anatase phase and rutile phase which exist in a tetragonal structure. The crystal form used as a photocatalyst is anatase and rutile phase, among these, an anatase phase is known to have excellent photolytic activity[33]. The crystal structure and physical properties of TiO_2 are shown in Fig. 3 and Table 4, respectively[32].

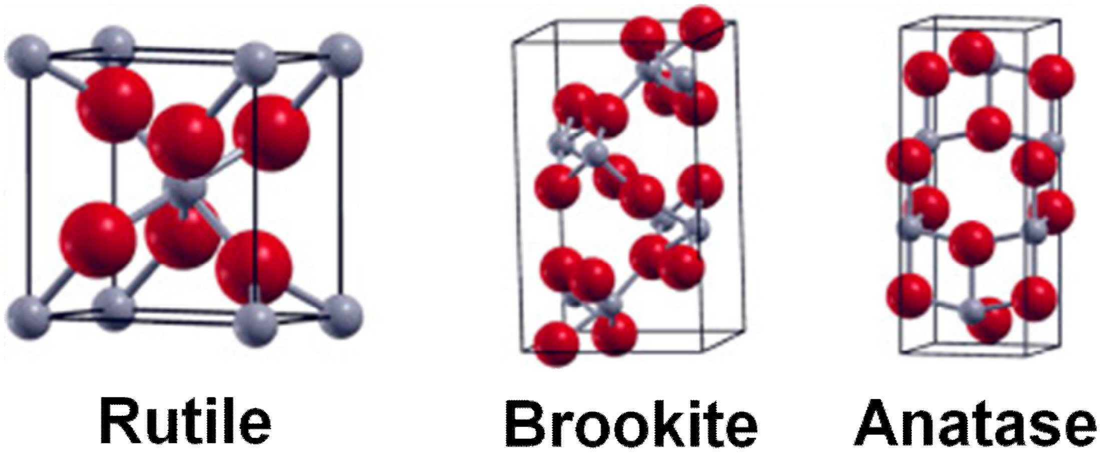

Fig. 3. Crystal structure of TiO_2[32].

Table 4. Physical properties of TiO_2[32)]

Property	Anatase	Rutile
Crystal structure	Tetragonal	Tetragonal
Atoms per unit cell (Z)	4	2
Space group	$l\frac{4}{a}md$	$P\frac{4_2}{m}nm$
Lattice parameters (nm)	a = 0.3785 c = 0.9514	a = 0.4594 c = 0.29589
Unit cell volume (nm^3)[a]	0.1363	0.0624
Density (kg m^{-3})	3894	4250
Calculated indirect band gap (eV)	3.23-3.59	3.02-3.24
(nm)	345.4-383.9	382.7-410.1
Experimental band gap (eV)	~ 3.2	~ 3.0
(nm)	~ 387	~ 413
Refractive index	2.54, 2.49	2.79, 2.903
Solubility in HF	Soluble	Insoluble
Solubility in H_2O	Insoluble	Insoluble
Hardness (Mohs)	5.5-6	6-6.5
Bulk modulus (GPa)	183	206

[a] Since the numbers of atoms per unit cell is halved upon going from rutile to anatase, the lattice parameters and unit cell volumes must be viewed accordingly.

2.4. Surface treatment for titanium[34)]

Ever since metal implants based on the osseointegration of the modern concept of 1969 were first practiced in Sweden, for the past 30 years Ti and Ti alloys have had the best clinical results. Ti and Ti alloys form a dense passive film on the surface, which is excellent in corrosion resistance and biocompatibility. However, since Ti does not have bioactive properties, it is slow in osteogenesis, has a long healing period, and has weak adhesion between bone and implant. In order to solve these drawbacks, studies have been carried out to increase the surface area of the implants, to change the surface shape, and to improve the bone bond strength through physical and chemical surface treatment. Since 1990, a variety of surface modification attempts have been made to increase the adhesion rate with bone tissue while minimizing the absorption of bone around the implant and to improve the affinity with the surrounding soft tissue and the bonding strength. Table 5 shows an overview of surface modification methods for Ti and its alloys implant[35)].

Table 5. Overview of surface modification methods for Ti and its alloys implants[35]

Surface modification methods	Modified lyaer	Objective
Mechanical methods		
Machining Griding Polishing Blasting	Rough or smooth surface formed by subtraction process	Produce specific surface topographies; clean and roughen surface; improve adhesion in bonding
Chemical method		
Chemical treatment		
Acidic treatment	< 10 nm of surface oxide layer	Remove oxide scale and contamination
Alkaline treatment	~ 1 μm of sodium titanate gel	Improve biocompatibility, bioactivity or bone conductivity
Hydrogen peroxide treatment	~ 5 nm of dense inner oxide and porous outer layer	Improve biocompatibility, bioactivity or bone conductivity
Sol-gel	~ 10 μm of thin film, such as calcium phosphate, TiO_2 and silica	Improve biocompatibility, bioactivity or bone conductivity
Anodic oxidation	~ 10 nm to 40 μm of TiO_2 layer, adsorption and incorporation of electrolyte anions	Produce specific surface topographies; improved corrosion resistance; improve biocompatibility, bioactivity or bone conductivity
CVD	~ 1 μm of TiN, TiC, TiCN, DLC thin film	Improve wear resistance, corrosion resistance and blood compatibility
Biochemical method	Modification through signalized titania, photochemistry, self-assembled monolayers, protein-resistace, etc.	Induce specific cell and tissue response by means of surface-immobilized peptides, proteins, or growth factors
Physical method		
Thermal spray Flame spray Plasma spray HVOF DGUN	~ 30 to 200 μm of coatings, such as Ti, HA, calcium silicate, Al_2O_3, ZrO_2, TiO_2	Improve wear resistance, corrosion resistance and biological properties
PVD		
Evaporation Ion plating Sputtering	~ 1 μm of TiN, TiC, TiCN, DLC, and HA thin film	Improve wear resistance, corrosion resistance, blood compatibility and biological properties
Ion implantation and deposition		
Beam-line ion implantation PIII	~ 10 nm of surface modified layer and/or ~ μm of thin film	Modify surface composition; improve wear, corrosion resistance, and biocompatibility
Glow discharge plasma treatment	~ 1 nm to ~ 100 nm of surface modified layer	Clean, sterilize, oxide, nitride surface; remove native oxide layer

2.4.1. Plasma electrolytic oxidation (PEO) process on Ti alloy

Ti implanted in the human body is brought into contact with the tissue by a thin oxide film, and this TiO_2 plays an important role in biocompatibility. The TiO_2 formed on the surface is excellent in corrosion resistance and durability against chemical substance, It can catalyze organic and inorganic chemical reactions, since it has a large dielectric constant, it can induce stronger Van der Waals forces than other oxides. Therefore, when the TiO_2 is artificially grown on the surface of the implant, the shape, thickness, and mixed elements greatly affect the reaction between the hard tissue.

PEO method is advantageous in that the thickness and shape of the TiO_2 can be easily controlled and reproducibility that more superior than the oxidation film formation method and the chemical oxidation method of heat treatment in the atmosphere. Local heating occurs at the defective area in the oxide film to cause breakdown, and as the high current flows through the electrode and the electrolyte, the heated electrolyte in the pore is captured, the high heat vaporized the electrolyte. Plasma composed of vapor and accelerating electrons ionized by electric discharge is formed in liquid state, and the ionized oxygen gas and the titanium combine to form an oxide film. Also, this phenomenon lasts on the surface of the entire TiO_2 as sparking continues around the pores where the breakdown has become a vulnerable part due to another defect or high heat. After the oxide layer is formed, an oxide film is repeated formation and destruction by plasma discharge. At this time, when the applied voltage is stopped, the surface roughness are increased and a non-uniform porous surface is obtained[34)].

During the PEO process, the main reactions leading to oxidation at the anode are as follows[35)]:

At the Ti/Ti oxide interface:

$$Ti \Leftrightarrow Ti^{2+} + 2e^{-}. \tag{1}$$

At the Ti oxide/electrolyte interface:

$$2H_2O \Leftrightarrow 2O^{2-} + 4H^{+} \tag{2}$$

(oxygen ions react with Ti to form oxide),

$$2H_2O \Leftrightarrow O_2\ (gas) + 4H^{+} + 4e^{-} \tag{3}$$

(O_2 gas evolves or stick at electrode surface).

At both interfaces:

$$Ti^{2+} + 2O^{2-} \Leftrightarrow TiO_2 + 2e^{-}. \tag{4}$$

In the PEO process, substances and surface shapes effective in covariance are added to the anodic oxide film as required according to the composition and concentration of the electrolyte, the temperature, the current density and the forming voltage structure favorable to physical bonding can be obtained, a structure favorable to physical bonding can be obtained, and chemical bonding can be induced through chemical components and tissue changes. Particularly, the separation phenomenon at the interface, which is a difficult point in the coating process, is not a problem because the anodic oxide coating is strongly chemically bonded[36-38].

2.4.2. RF-magnetron sputtering using physical vapor deposition (PVD)[39]

Methods for forming thin films and nanostructure include PVD and CVD methods. PVD is usually used to make high-quality thin films or nanostructures, and since the vacuum environment is required, it is expensive equipment, when rapid deposition on a large area, the CVD method is used. In general, PVD methods are used to obtain better quality deposition surfaces.

Examples of the vapor deposition method corresponding to PVD include sputtering, electron beam vapor deposition, thermal vapor deposition, laser molecular vapor deposition, and pulse laser vapor deposition. Of these, sputtering is the most effective method for improving corrosion resistance of thin films and nanostructures. Such a sputtering method is classified into DC sputtering, RF sputtering, and magnetron sputtering, and In the case of DC sputtering, when the cathode is impacted by ions, Since electrons are lost from the cathode surface, in case of the electrode becomes an insulating layer, the glow discharge cannot be maintained at the DC voltage. Therefore, lost electrons can not be replaced. This cathode surface decreases the potential difference, and in case of the cathode is an insulator, ions will accumulate because electrons cannot be provided. Because of this the insulator is not sputtered.

For Ar^+ in DC-sputtering:

$$Ar^+ + e^- \rightarrow Ar \tag{5}$$

When this accumulation occurs, the Ar^+ ions do not collide with each other due to the + charge accumulated on the target and the electrostatic repulsion, so that they can not be sputtered.

To sustain a glow discharge using an insulator target, replace the DC power supply with an RF power supply, and Impedance matching network must be implemented. The RF sputter prevents the accumulation of charge on the target surface by continuously changing the polarity of the applied voltage, and sputtering of non-metals, insulators, oxides, and dielectrics other than metals is possible. A target to which a permanent magnet is attached to a cathode and which applies a magnetic field in a direction parallel to the target surface is called a magnetron target, and since the magnetic field is parallel to the target surface, it is perpendicular to the electric field. Therefore, the electrons receive the force of Lorentz, and they are spiraling movement because they are accelerated by the turning motion. Prevent not electrons to escape near the target, and because the electron keeps turning in, around, the plasma is kept very close to the target, and as the plasma density increases in the nearby region, the ion exchange rate increases.

When magnetron sputtering is sputtered using a metal target, by simultaneously flowing the inert gas (Ar^+), when a (-) voltage is applied to the cathode, the electrons emitted from the cathode collide with the Ar gas atoms, and It is mainly used to form a compound thin film by ionizing Ar.

For Ar^+ in RF-sputtering:

$$Ar + e^- \text{ (primary)} = Ar^+ + e^- \text{ (primary)} + e^- \text{ (secondary)} \qquad (6)$$

Fig. 4 is a Schematic diagram of the physical release principle of the sputter system. During magnetron sputtering on any material, the thin film is formed in the form of a solid solution alloy, a compound, or a mixture of the two, in which particles of the reactive gas (Ar^+) are mixed in the metal thin film.

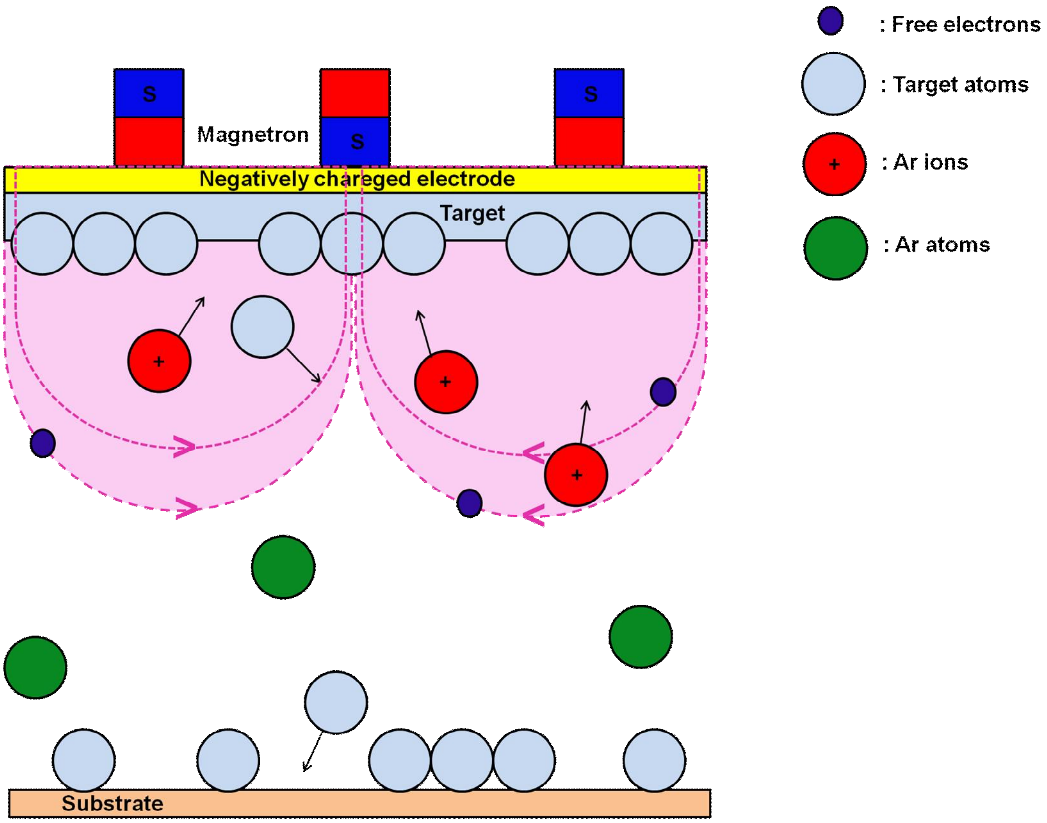

Fig. 4. Schematic diagram of the physical release principle of the sputtering system[39].

2.4.3. Zinc (Zn)

It is known that zinc (Zn), strontium (Sr), magnesium (Mg), sodium (Na), silicon (Si), silver (Ag) and yttrium (Y) which constitutes the human body, plays an important role in bone formation because it affect bone density. The role of each ion in the human body, as shown in Table 6[40-42]. In particular, ZnO is used as a source of Zn, which serves important and critical roles in growth, development and well-being in humans and animals[43]. ZnO can present three crystal structures: Wurtzite, zinc blende and rocksalt, as shown in Fig. 5. At ambient conditions, the thermodynamically stable phase is the Wurtzite structure, in which every Zn atom is tetrahedrally coordinated with four oxygen atoms[43]. As a result of previous research[43] have tested the in vitro antibacterial activity of ZnO, using pure nanoparticles or nanoparticle suspensions, also known as nanofluids. These ZnO has shown antimicrobial activity against Gram-negative bacteria such as Pseudomonas aeruginosa, Campylobacter jejuni and Escherichia coli. Recently, the preparation of Zn-substituted microporous films and the formation and growth of microporous film crystals have been studied[12,13,15,36-38]. Zn is known as a calcium substitute because it has a structure in which the cation lattice structure of HA can be easily substituted with various elements. In this case, the particle shape, lattice size, crystallinity, and thermodynamic characteristics of the powder are influenced, and cation (Zn^{2+}, Mg^{2+}, Sr^{2+}) and anion (SiO_4^{4-}, F^-, CO_3^{2-}) are mainly used as substitution ions[44]. In addition, Zn is one of the major substitution ions of calcium, and the amounts contained in enamel, dentine, and bone are 263 ppm, 173 ppm, and 39 ppm, respectively, and the eighth most abundant cation in the extracellular temperament of bone[45]. Table 7 shows the comparative composition of enamel, dentine, and bone. Zn deficiency reduces nucleic acid metabolism, proteinogenesis and bone growth and activity in vivo, thereby increasing the functionality of the fracture.

Therefore, it is expected that the addition of Zn in the Ca-deficient HA lattice affects the Ca/P ratio, thereby facilitating the formation of β-TCP and thus having excellent biocompatibility and having characteristics comparable to hard tissue[12]. The following steps represent the chemical modification reaction sequence for the substitution of the Ca and Zn ions, noting that $Zn_3(PO_4)_2 \cdot 4H_2O$ is the main component of the Zn-Ca-P coating[46].

$$Ca^{2+} + HPo_4^{2-} \rightarrow CaHPO_4 \quad (7)$$

$$3CaHPO_4 \rightarrow Ca_3(PO_4)_2 + H_3PO_4 \quad (8)$$

$$3Zn^{2+} + 2H_2PO_4^{-} + 2H^{+} + 4H_2O + 6e \rightarrow Zn_3(PO_4)_2 \cdot 4H_2O + 3H_2\uparrow \quad (9)$$

Table 6. Effect of selected metallic ions on human bone metabolism and angiogenesis summary of literature studies[40-42]

Ion	Biological response in vivo / in vitro
Si	● essential for metabolic processes, formation and calcification of bone tissue ● dietary intake of Si increases bone mineral density (BMD) ● aqueous Si induces HAp precipitation ● $Si(OH)_4$ stimulates collagen I formation and osteoblastic differentiation
Ca	● Favours osteoblast proliferation, differentiation and extracellular matrix (ECM) mineralization ● activates Ca-sensing receptors in osteoblast cells, increases expression of growth factors, e.g. IGF-I or IGF-II
P	● stimulates expression of matrix la protein (MGP) a key regulator in bone formation
Zn	● shows anti-inflammatory effect and stimulates bone formation in vitro by activation protein synthesis in osteoblasts ● increases ATPase activity, regulates transcription of osteoblastic differentiation genes, e.g. collagen I, ALP, osteopontin and osteocalcin
Mg	● stimulates new bone formation ● increases bone cell adhesion and stability (probably due to interactions with integrins)
Sr	● shows beneficial effects on bone cells and bone formation in vivo ● promising agent for treating osteoporosis
Cu	● significant amounts of cellular Cu are found in human endothelial cells when undergoing angiogenesis ● promotes synergetic simulating effects on angiogenesis when associated with angiogenic growth factor FGF-2 ● stimulates proliferation of human endothelial cells
B	● induces differentiation of mesenchymal cells towards the osteogenic lineage ● stimulates RNA synthesis in fibroblast cells ● dietary boron stimulates bone formation

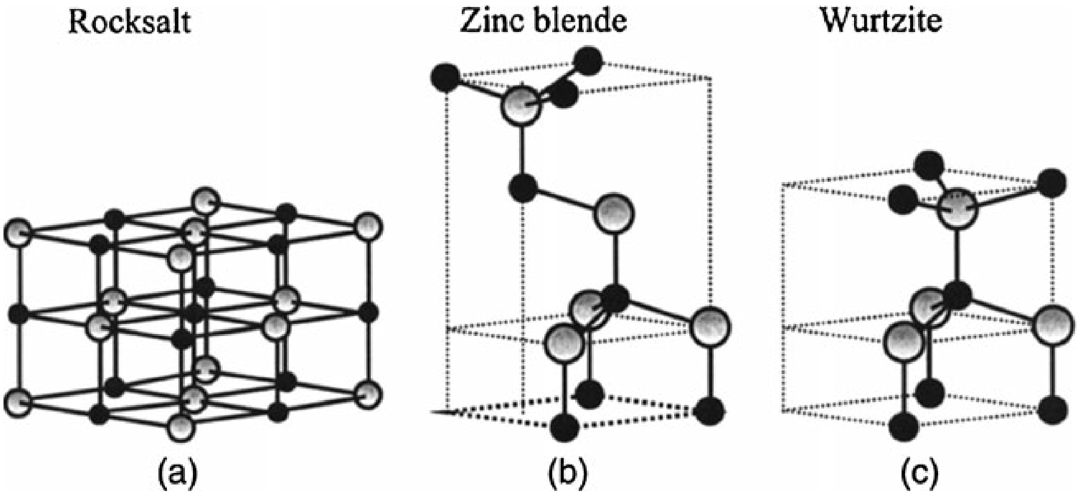

Fig. 5. ZnO crystal structures: cubic rocksalt (a), cubic zinc blende (b), and hexagonal Wurtzite (c). The shaded gray and black spheres represent zinc and oxygen atoms[43].

Table 7. Comparative composition of human enamel, dentin, and bone[45]

	Enamel	Dentine	Bone
Ca (wt.%)	37.6	40.3	36.6
P (wt.%)	18.3	18.6	17.1
Co_2 (wt.%)	3.0	4.8	4.8
Na (wt.%)	0.70	0.1	1.0
K (wt.%)	0.05	0.07	0.07
Mg (wt.%)	0.2	1.1	0.6
Sr (wt.%)	0.03	0.04	0.05
Cl (wt.%)	0.4	0.27	0.1
F (wt.%)	0.01	0.07	39.0
Zn (ppm)	263.0	173.0	
Ba (ppm)	125.0	129.0	
Fe (ppm)	118.0	93.0	
Al (ppm)	86.0	69.0	
Ag (ppm)	0.6	2.0	
Cr (ppm)	1.0	2.0	0.33
Co (ppm)	0.1	1.0	< 0.025
Sb (ppm)	1.0	0.7	
Mn (ppm)	0.6	0.6	0.17
Au (ppm)	0.1	0.07	
Br (ppm)	34.0	114.0	
Si (ppm)			500
Ca/P	1.59	1.67	1.65

III. MATERIALS AND METHODS

3.1. Preparation of samples

Ti-6Al-4V ELI disk (grade 5, Timet Co. Ltd, Japan) with diameter; 10 mm, thickness of 3 mm was as substrate sample in the study. The pre-treatment of samples was conducted as follows; polishing with 100 - 2000 grit sandpaper, rinsing in distilled water and ultrasonically cleaning in ethyl alcohol for 10 min.

3.2. PEO treatment on the alloy surface

Pre-treated samples were used as anodes (sample name: Ca/P) and Pt rod was used as cathode in different electrolytic bathes as shown in Table 8. The schematic diagram of PEO treatment system is shown in the Fig. 6. Electrolytes were used for 0.15 M calcium acetate + 0.02 M calcium glycerophosphate for PEO process.

A pulsed DC power supply (KEYSIGHT Co., Ltd.; USA) was employed for PEO process. The optimum applied voltage and PEO-treated time were selected to be 280 V and 3 min, respectively. The temperature of the electrolyte was kept below 25 °C by a cooling system. The PEO-treated samples were rinsed with distilled water, and then dried using warm air.

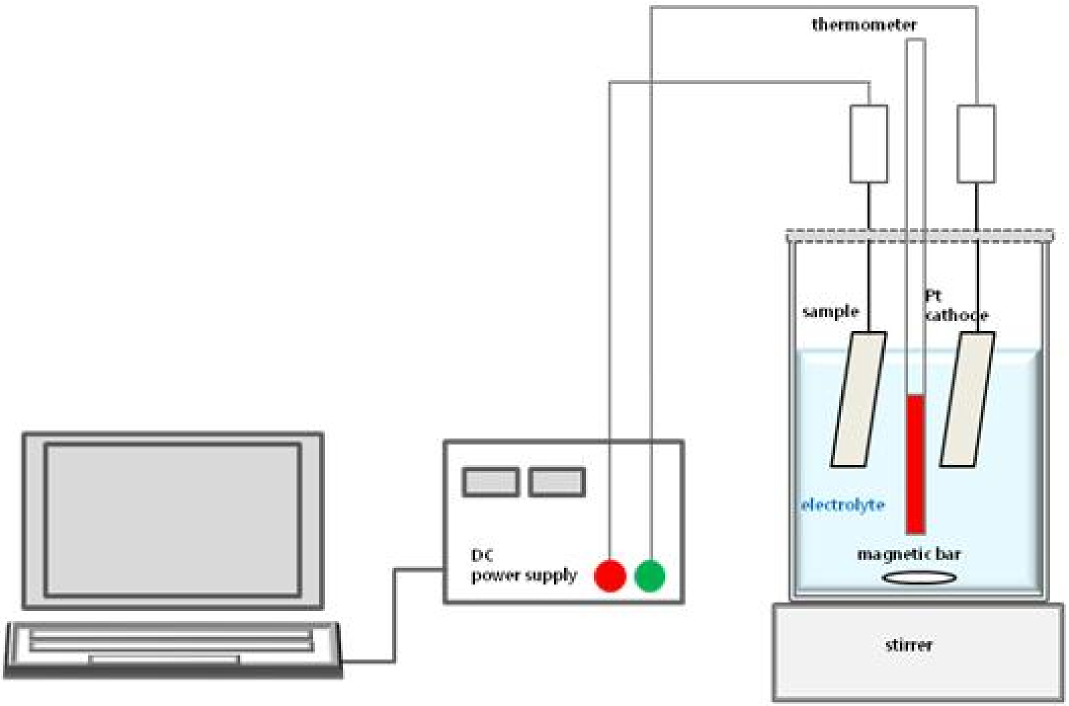

Fig. 6. Schematic diagram of PEO treatment system.

Table 8. The condition of electrochemical deposition

Working equipment	DC Power supply (KEYSIGHT Co., Ltd.; USA)
Working electrode	Sample (Ti-6Al-4V alloys)
Counter electrode	High dense carbon
Electrolyte	0.15 M Calcium acetate monohydrate [$C_4H_6CaO_4 \cdot H_2O$] + 0.02 M Calcium glycerophospate [$C_3H_7CaO_6P$]
Applied voltage	280 V
Applied current	70 mA
Time	3 min

3.3. Zinc coating by the radio-frequency (RF) magnetron sputtering

The Zn thin film was coated using a RF-magnetron sputtering system (A-Tech system Co., Korea). The schematic diagram of RF-magnetron sputtering system is shown in Fig. 7. And the condition for Zn coating is shown in Table 9. The distance between the substrate and the target was 80 mm, and Zn target with a diameter of 4 inch was used for sputtering. The pressure in the chamber was initially set to less than 10^{-6} Torr. A mass flow controller was used to generate a 40 sccm argon (Ar) gas flow into the chamber. The coating pressure of the Ar gas atmosphere was maintained at $2.0 \sim 4.0 \times 10^{-2}$ Torr, and a RF power of 60 W was applied for 0, 1, and 3 min (sample name: Ca/P for 0 min, 1 min/Zn for 1 min, 3 min/Zn for 3 min), which led to the formation of plasma. Prior to coating, pre-sputtering was carried out with Ar gas using a shield to protect the sample for 5 min.

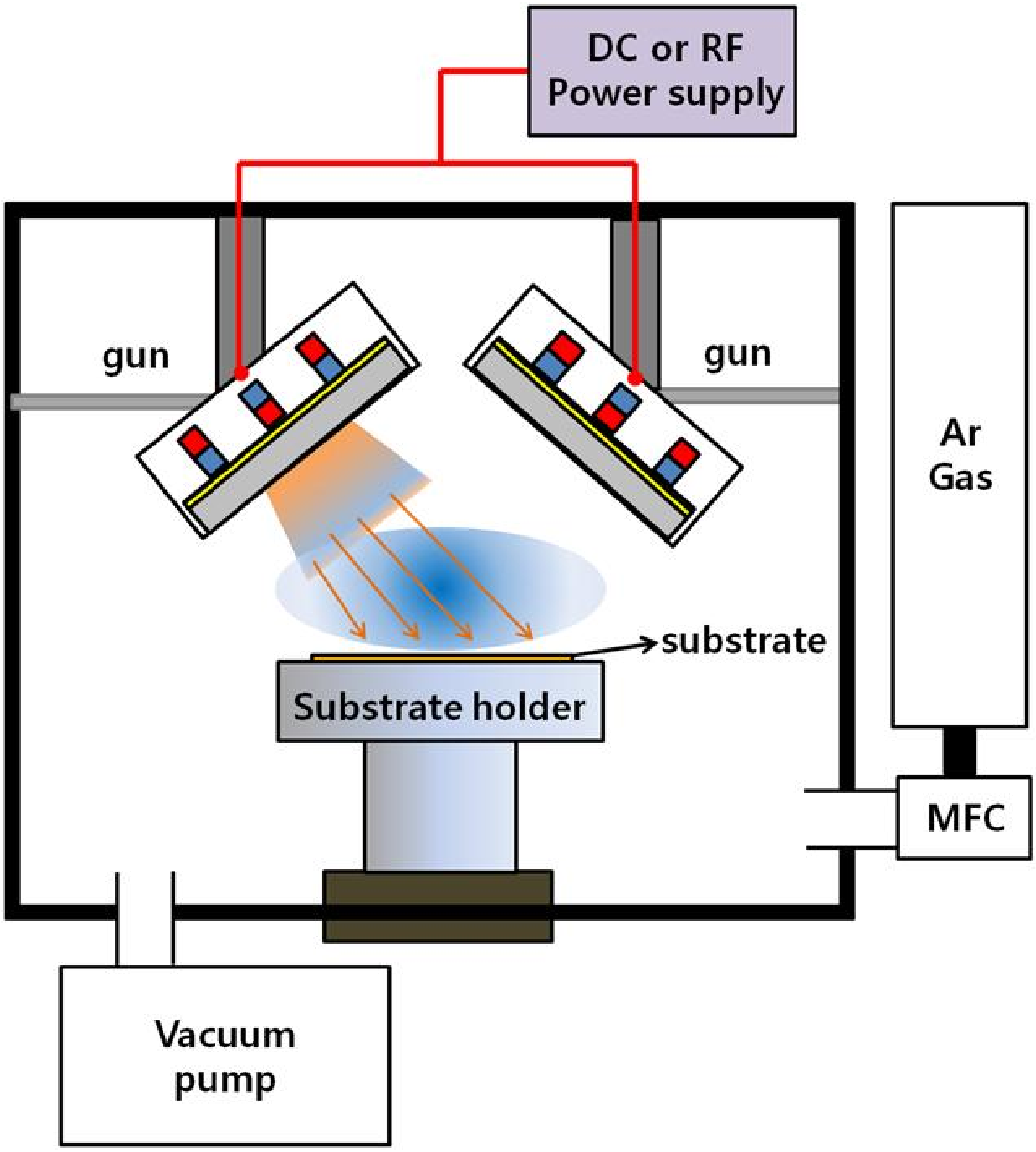

Fig. 7. Schematic diagram of RF-magnetron sputtering system.

Table 9. The coating condition of RF-magnetron sputtering

Coating condition	TiO_2 film
Equipment	RF sputtering
Target	Zn (99.99%)
Base pressure	10^{-6} Torr
Working pressure	10^{-3} Torr
Gas	Ar (40 sccm)
Pre-sputtering	10 min
Deposition time	0, 1, 3 min
Power supply	60 W

3.4. Surface characterization for Ti-6Al-4V alloys

To RF-sputtered Zn coatings on PEO-treated sample surfaces were characterized by using a field-emission scanning electron microscopy (FE-SEM, S-4800, Hitachi Co., Japan), and thin-film X-ray diffractometer (TF-XRD, X'pert Pro MPD, PANalytucal Co., Netherlands) with Cu K_α radiation. Energy dispersive X-ray spectroscopy (EDS, E-MAX, Horiba Co., Japan) was used to analyze the Ca, P, and Zn in the RF-sputtered Zn coating surface after PEO treatment.

3.5. Cell culture test

MC3T3-E1, an osteoblast-like cell line, was extracted from a mouse skull was appropriately dispensed at a concentration of 1×10^6 cells / ml. Cells were cultured in α-MEM (α-minimum essential medium) medium supplemented with 10 % fetal bovine serum (FBS), 10 U/㎖ penicillin/streptomycin. The cells were cultured at 37 ℃ and 5 % CO_2 continuously, and the culture medium was changed every 2~3 days until sufficient growth of the cells occurred. Cells were seeded on a 12 well-plate at a concentration of 1×10^5 cell/㎖, and after incubation at 37 ℃ for 24 h. To observe cell attachment pattern by FE-SEM, the cells were washed 3 times with PBS (phosphate buffer saline) and fixed with 2.5 % glutaraldehyde solution for 2 h. After that, cell were dehydrated as from 40 % to 100 % increased by 10 % every 15 minutes of mixture solution of ethanol and distilled water at room temperature.

Ⅳ. RESULTS AND DISCUSSION

4.1. Surface characterization of RF-sputtered Zn coatings on PEO-treated Ti-6Al-4V alloys

Formation of a porous oxide film according to the PEO method is an effective method for producing an Hydroxyapatite (HA) layer. Being formed the irregular TiO_2 layer, the HA coating on the surface formed in the pores improves implant surface for osteoblast adhesion on the surface. Success of implant surgery depends on the formation of surrounding osseointegration. The contact surface between the implant interface and the bone is very important. Therefore, to obtain sufficient contact with the bone after implantation is essential to improve the biocompatibility of the implant by increasing the surface area of the implant. The rough surface formed by surface treatment is well formed osseointegration and cell morphology and growth. In addition, recent studies on Zn-doped HA films have attracted much attention due to good biocompatibility. Based on these results, It tried to improve the biocompatibility by using PEO treatment and Zn-coating.

Fig. 8 shows FE-SEM images of the RF-sputtered Zn coatings on PEO- treated on Ti-6Al-4V alloys for various sputtering time. Fig. 8 (a, a-1, and a-2) shows the PEO-treated surface in electrolyte containing Ca and P ions at 280 V. Fig. 8 (b, b-1, and b-2) and (c, c-1, and c-2) shows Zn coated surface with various sputtering time: 1 min and 3 min, respectively. The surface of oxide films by typical of samples after PEO coating showed formation of many micro-pores with uniform distributions. Although the RF-sputtering was carried out after PEO-treated surface, the morphology of RF-sputtered was not different from PEO-treated surface with low magnification. All the morphologies of RF-sputtered surface showed the small particles covered with droplet shape on the pore inside and surface parts. Especially, the surface part showed many numbers of particles compared to pore inside. As the sputtering time increased, the circular particles of Zn coatings on the Ti-6Al-4V alloys increased at pore inside and surface parts. In addition, in case of morphology of Zn coated micro-pore on Ti-6Al-4V alloys by electrochemical method, circular particle appear to be more distinct. And all the morphologies of Zn coatings on the micro-pore formed Ti-6Al-4V alloys showed many circular particles at surface part. It is confirmed that these droplet particles in the sputtering process are formed with the bombardment of the substrates by energetic particles[47)].

Fig. 9 shows the content of Ca, P, and Zn with Zn-sputtering time on PEO-treated Ti-6Al-4V alloys for pore inside and surface part in the EDS results of point analysis. According to EDS results, surface of RF-sputtered Zn coating on Ti-6Al-4V alloys were covered entirely with the Zn film. It should be noted that the [Ca+Zn]/P ratio for the Zn coating on the PEO-treated Ti-6Al-4V alloys of the surface was 1.59, 1.63, and 4.92 for low-magnification total area as shown in Fig. 10. As the sputtering time increased, [Ca+Zn]/P ratio for the RF-sputtered Zn coatings after PEO-treated on Ti-6Al-4V alloys were increased with Zn content as shown in EDS analyses of Table 10. This is probably due to the increased Zn content on the surface by sputtering. Therefore, when the sputtering time is increased, the Ca/P ratio is almost the same as the bone but the [Ca+Zn]/P ratio is greatly increased by the increase of Zn content. In addition, it assumed that growing in perpendicular direction of sputtering coated layer was confirmed at substrate of columnar structure.

Fig. 11, 12, and 13 show the EDS mapping for distributions of implanted elements on the PEO-treated surface and contented elements on the Zn-coating after PEO-treated Ti-6Al-4V alloys. For the Ti-6Al-4V alloys modified with Ca/P and Zn coating, the surface of the micro-pore structure was completely covered and as the sputtering time was longer, the EDS mapping data for Zn coating at Ti-6Al-4V confirmed the uniform distribution of large amounts of Zn. In addition, less distribution of Zn was detected within the pore inside than on the surface part. Thus, it is determined that Ca, P, and Zn undergo uniform distribution over the entire crystal particles upon the substitution of Ca with Zn. It is thought that Zn increases the biocompatibility and mitigates bone reaction in the implant surface. The release of Zn in the body is strongly mediated by the bone reservoir, and Zn incorporation into implants may promote bone formation on the implant surface[48].

Fig. 14 shows the TF-XRD peaks of the RF-sputtered Zn coatings on the PEO-treated Ti-6Al-4V alloys in order to observe the formation of oxide film and crystallinity at various sputtering times. In case of PEO-treated sample and Zn coatings after PEO-treated Ti-6Al-4V alloys, peaks showed at 25 ° , which was confirmed to be anatase crystal phase which is one of TiO_2 crystal phases, in comparison with JCPDS (Joint Committee on Powder Diffraction Standards, PCPDFWIN) #21-1272. Additionally, 27 ° of peak can be observed, which is a rutile structure, which is another crystal phase of TiO_2, which could be confirmed by the JCPDS #21-1272. As the sputtering time became longer, it was observed that the amorphous peak was increased, whereas crystal phase was decreased. The position of anatase peak was shifted slightly to a lower angle, in the case of Zn coating on the Ti-6Al-4V alloys in Fig 14; antase peak of Ca/P (2θ = 25.40 °), 1 min/Zn (2θ = 25.38 °), and 3 min/Zn (2θ = 25.38 °), respectively. The shifted peaks can be appeared in the case of increased internal distortion. Therefore, It is thought that shifted peaks of anatase is occurred due to distortion of titanium oxide films for PEO and sputtering process. In addition, It is considered that HA-α crystal phase is increased, which leads to thinning of the oxide film[49]. Through the experiment, it could confirm that the Zn-sputtering time affect the crystallinity of Zn coatings[50,51]. That is, Zn coatings showed the amorphous structure from Fig. 14(d). Also, in order to find out the crystallite size on the surface, using the anatase peak formed on surface of Zn-sputtering on PEO-treated Ti-6Al-4V alloy as shown in Table 11, the crystallite size at the diffraction angle ofanatase peak are calculated as Scherrer's equation[52].

$$D = \frac{0.9\lambda}{\beta\cos\theta} \tag{10}$$

where D is the diameter of crystallites, B is the full width at half-maximum peak intensity (FWHM: radians), θ is the angle of incidence for the X-rays (Bragg angle), and λ is the X-ray wavelength (Cu Kα: λ = 0.15406 nm). According to the values calculated by the equation, the FWHM and crystallite size (nm) of the anatase phase with respect to the Zn-sputtering time after the PEO treatment in the Ti alloy were 4.32×10^{-3} and 1.73 / 6.59×10^{-3} and 1.66 / 5.46×10^{-3} and 2.00, respectively. These results indicated that the crystallite size increased due to localized heating when the surface was exposed to plasma in the solution at high voltage[53].

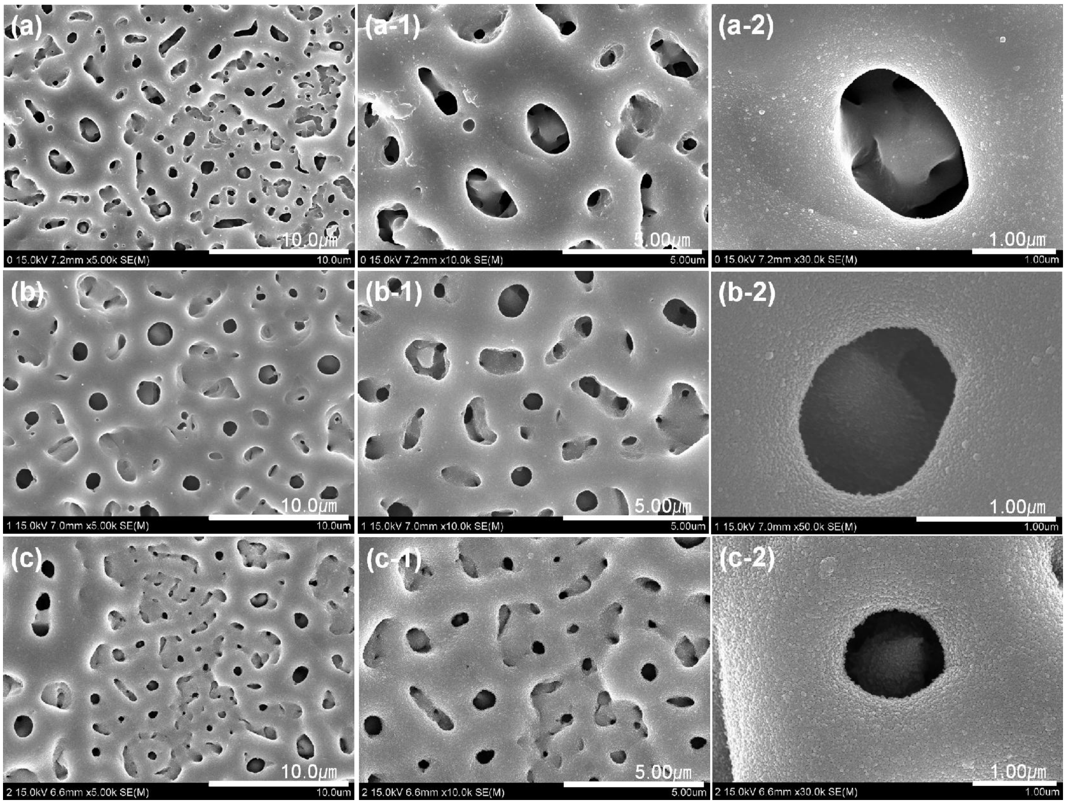

Fig. 8. FE-SEM images of the RF-sputtered Zn coating on PEO-treated Ti-6Al-4V alloys for various sputtering time:

(a) PEO-treated surface in electrolyte containing Ca and P ions,

(b) Zn coated surface for 1 min,

(c) Zn coated surface for 3 min,

(a-1) 10,000 magnification of (a), (a-2) 30,000 magnification of (a),

(b-1) 10,000 magnification of (b), (b-2) 30,000 magnification of (b),

(c-1) 10,000 magnification of (c), and (c-2) 30,000 magnification of (c).

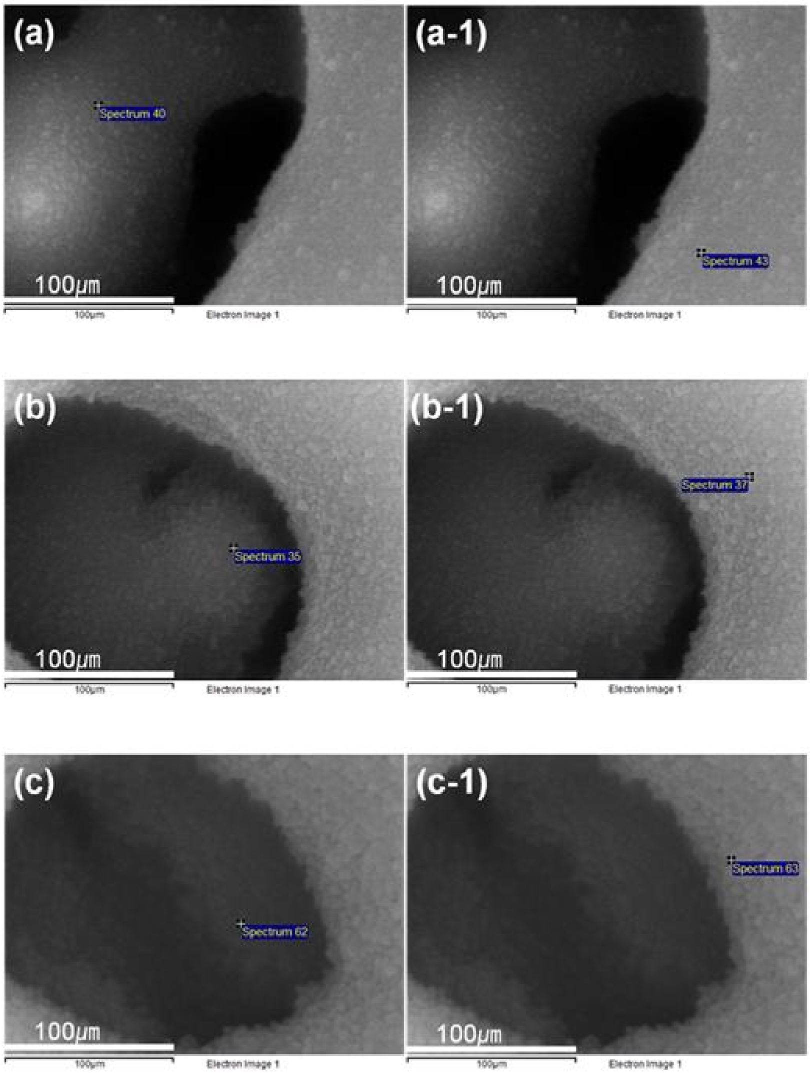

Fig. 9. FE-SEM images and EDS analyses of the RF-sputtered Zn coating on PEO-treated Ti-6Al-4V alloys for pore inside and surface part:
(a) PEO-treated surface in electrolyte containing Ca and P ions at pore, (b) Zn coated surface for 1 min at pore, (c) Zn coated surface for 3 min at pore, (a-1) PEO-treated surface in electrolyte containing Ca and P ions at surface, (b-1) Zn coated surface for 1 min at surface, and (c-1) Zn coated surface for 3 min at surface.

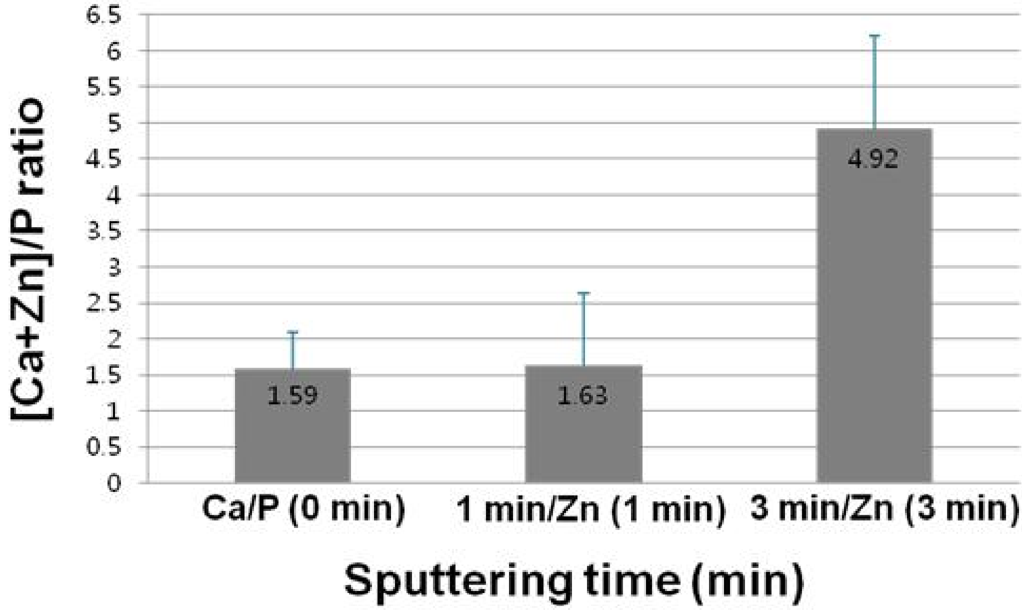

Fig. 10. Variation of [Ca+Zn]/P ratio with RF-sputtering time on PEO-treated Ti-6Al-4V alloys.

Table 10. EDS analysis results of pore inside and surface part

Samples (wt.%) / Elements	Ca/P		1Min/Zn		3Min/Zn	
	pore	surface	pore	surface	pore	surface
O K	20.99	44.41	32.32	42.61	14.16	36.82
Al K	2.42	2.58	2.18	2.77	1.47	2.17
P K	7.08	6.75	7.08	7.85	5.58	4.66
Ca K	8.75	7.46	8.86	8.49	5.79	4.68
Ti K	56.51	36.43	45.58	33.22	52.04	30.95
V K	4.25	2.37	1.59	1.00	2.99	2.30
Zn K	-	-	2.39	4.06	17.97	18.42
Total	100.00					

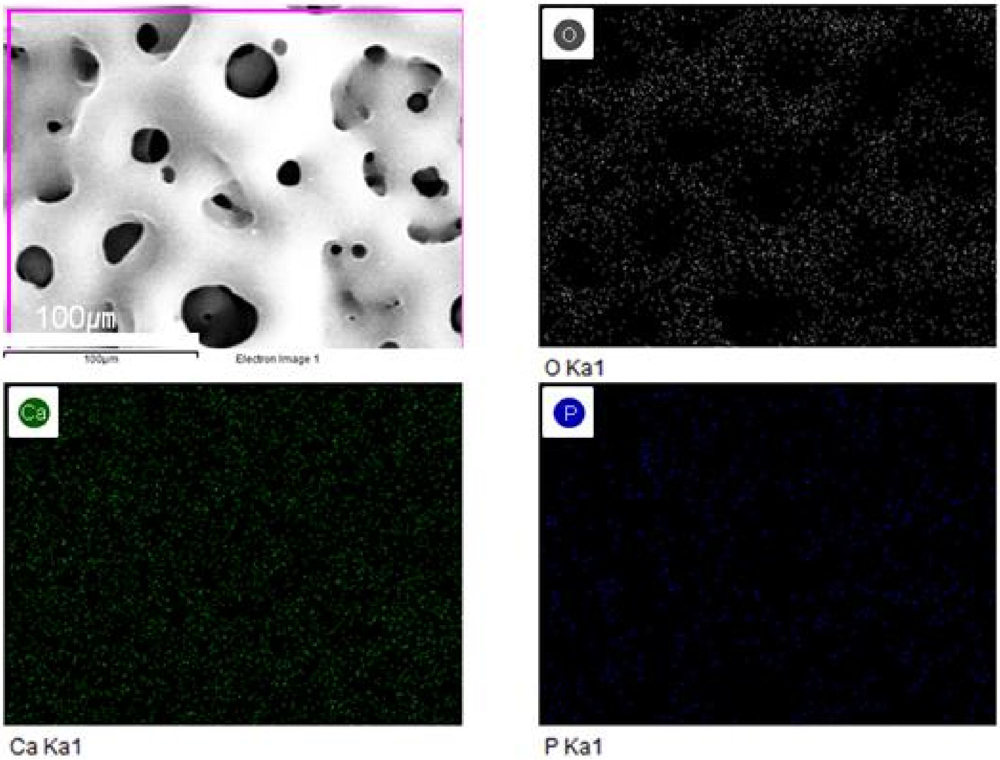

Fig. 11. EDS mapping images of the PEO-treated Ti-6Al-4V alloys in electrolyte containing Ca and P.

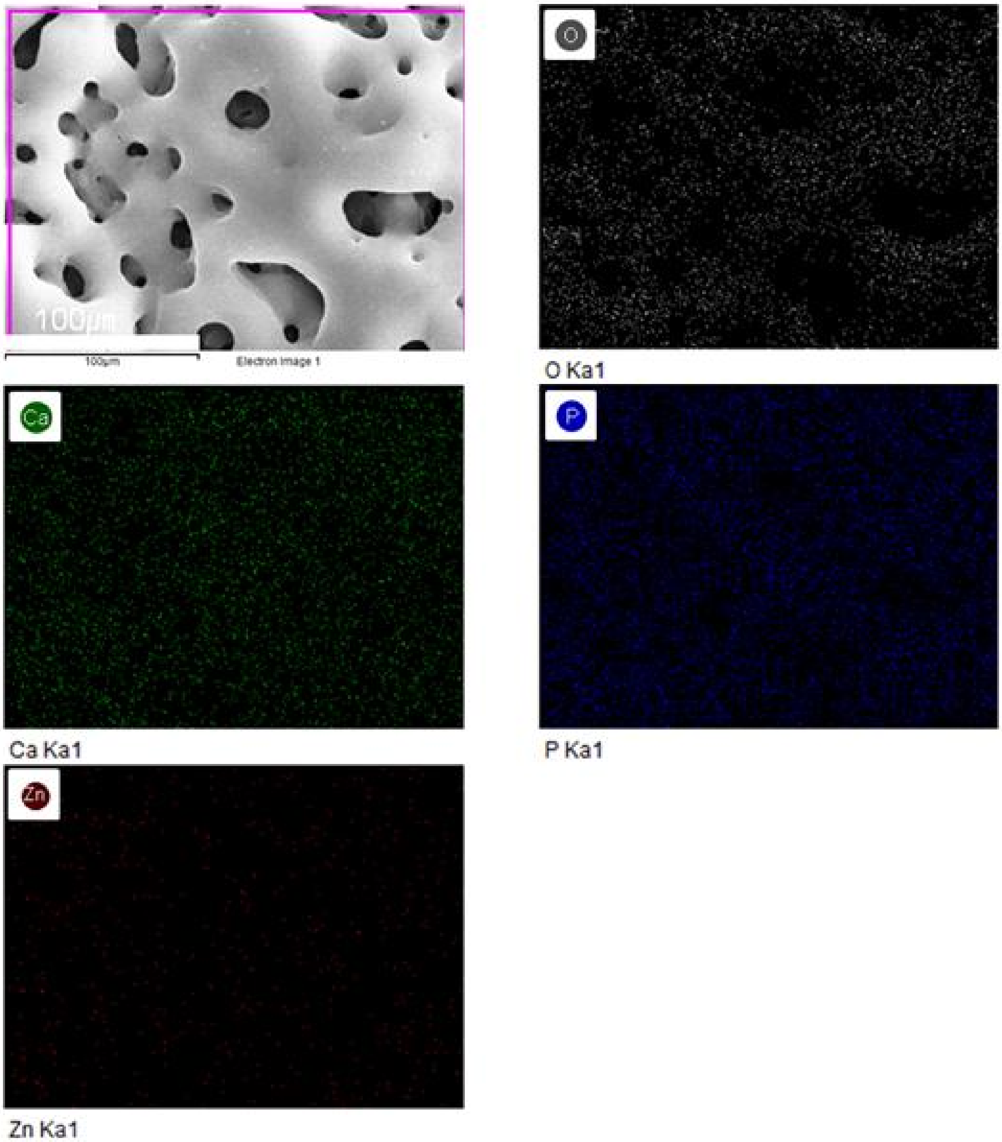

Fig. 12. EDS mapping images of the RF-sputtered Zn coating on PEO-treated Ti-6Al-4V alloys for 1 min/Zn coating.

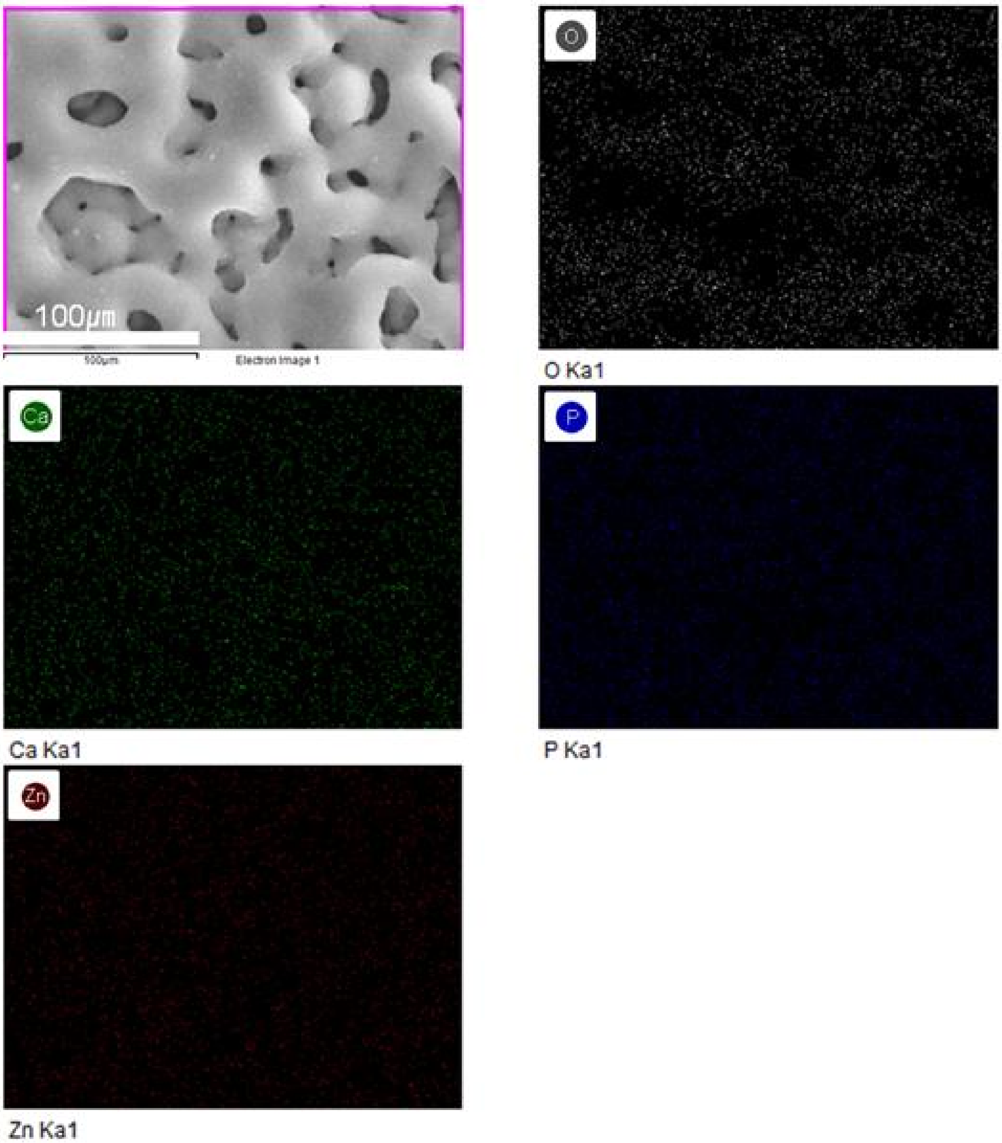

Fig. 13. EDS mapping images of the RF-sputtered Zn coating on PEO-treated Ti-6Al-4V alloys for 3 min/Zn coating.

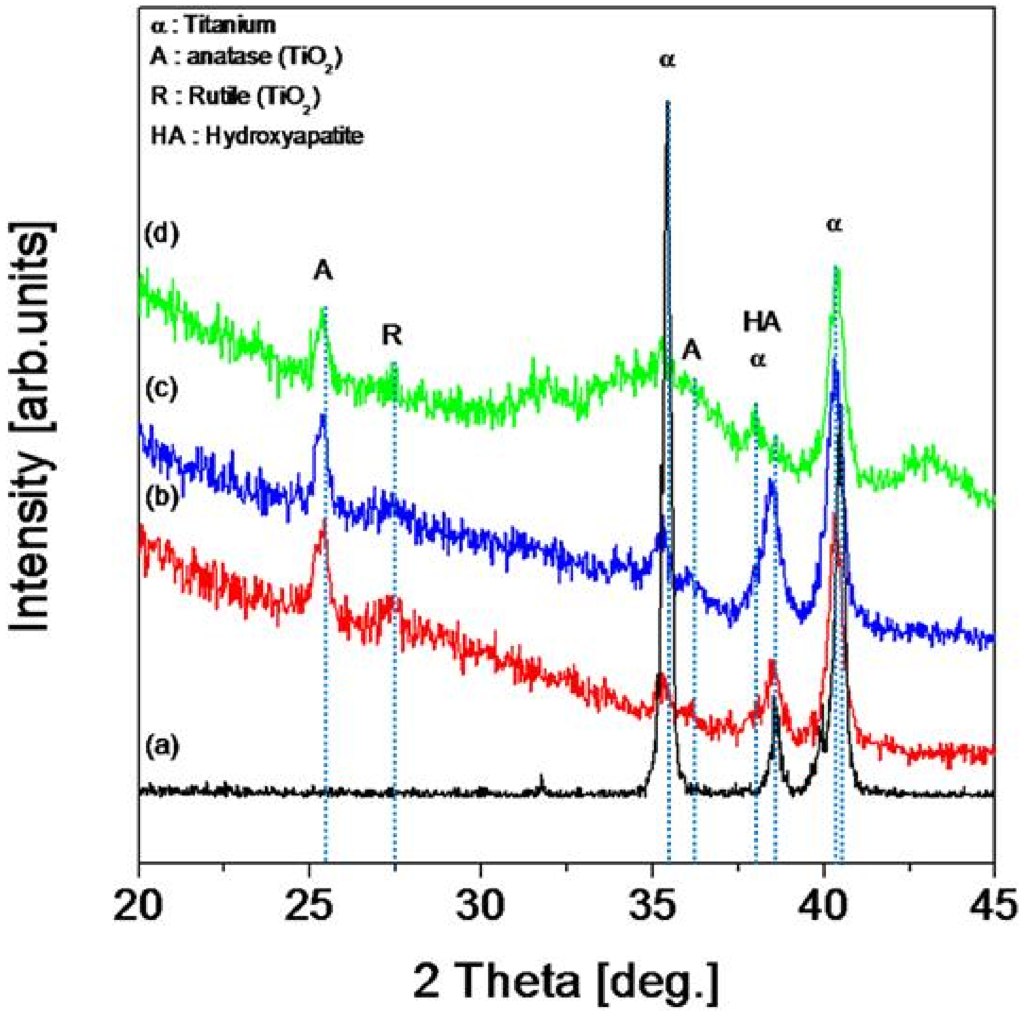

Fig. 14. XRD spectra of the RF-sputtered Zn coating on PEO-treated Ti-6Al-4V alloys in various sputtering time: (a) Ti-6Al-4V, (b) Ca/P, (c) 1 min/Zn coating, and (d) 3 min/Zn coating.

Table 11. The variation of crystallite size with Zn-sputtering time on PEO-treated surface

anatase phase / Zn-sputtering time	Diffraction angle (2Θ)	FWHM (radian)	Crystallite size(t)
Ca/P	25.40	4.32×10^{-3}	1.73
1min/Zn	25.38	6.59×10^{-3}	1.66
3min/Zn	25.38	5.46×10^{-3}	2.00

4.2. *In vitro* evaluation using MC3T3 cells

Fig. 15 is a FE-SEM images of MC3T3-E1 osteoblast cells grown on various surface-treated Ti-6Al-4V alloys surfaces at 37 ℃ for 24 h. For the experimental group, surface treated samples (PEO-treated and Zn coating on PEO-treated samples) were used and bulk samples were used as a control group. As a result, cell proliferation and differentiation were observed more actively in the experimental group than in the control group. In the case of bulk samples, the number and growth of cells were slow, whereas in surface-treated samples, cells grew in various forms. In particular, lamellipodia and filopodia growth were observed in various directions in Ca/P and 1 min/Zn coated samples, in general, filopodia are well adhered to the inside of pores in 1 min/Zn and 3 min/Zn samples with micro/nano-shapes except for bulk which has un-treatment on the alloy.

This was followed by MTT assay, which is directly related to cell viability and mitochondrial activity. The evaluation of MC3T3-E1 osteoblasts cell adhesion and proliferation on the surface of the control and experimental groups was made by MTT assay. The un-treated bulk was used as a control group, Ca/P, 1 min/Zn and 3 min/Zn coated surfaces were used as experimental groups at the same conditions, and cell viability as shown in Fig 16. MTT analysis showed that the surface of PEO-treated and Zn coating showed higher survival rate than the un-treated surface, and the surface of 1min/Zn-sputtered showed the highest survival rate at 103.02 %. In particular, Zn-contained surfaces showed better cell differentiation and survival rates. According to previous study[43,54,55], Zn-implanted titanium presented partly antibacterial effect on both *E. coli* and *S. aureus*, and it stimulates proliferation, early attachment and spreading activity of osteoblastic MC3T3-E1 cells did[43,54,55]. This suggested that the initial adhesion and growth of cells were strongly dependent on surface roughness. It can be seen that the coexistence of micro-pores, nano-surfaces and bioactive elements contained Zn sputtering particles was maximized compared to the case where only micropores exist[56,57].

As a result of the study, the surface of Ti-6Al-4V alloys coated with Zn for 1 min by sputtering showed a good biocompatibility.

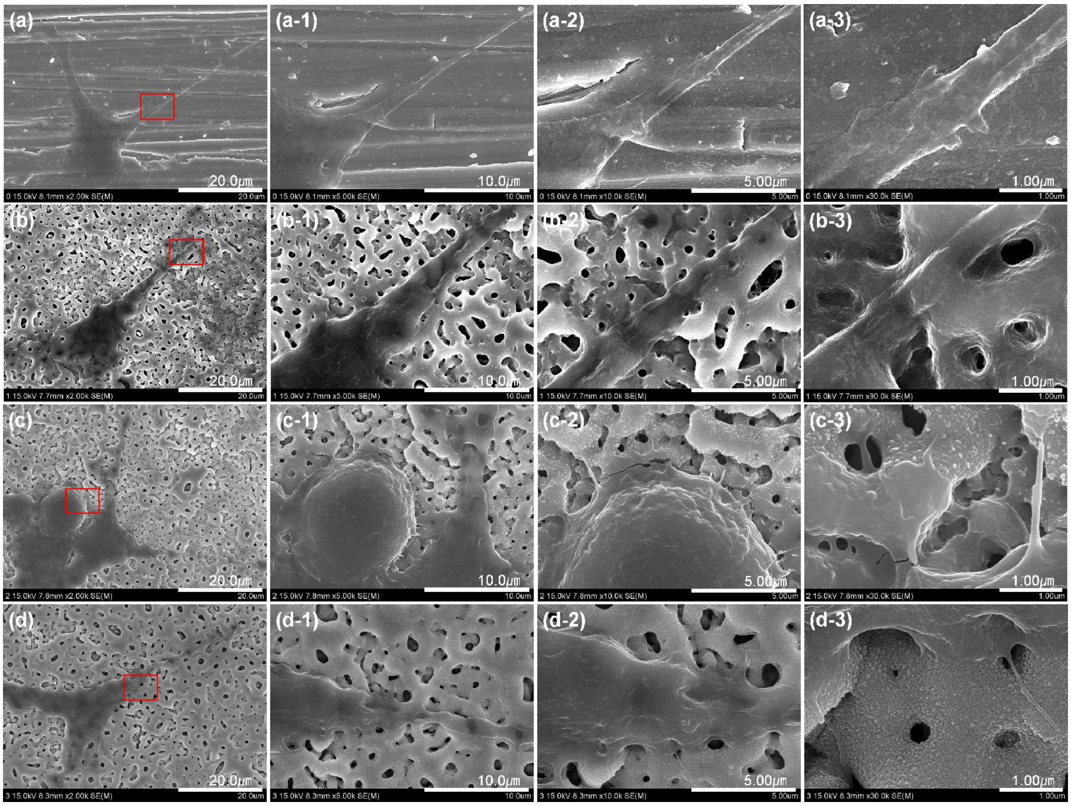

Fig. 15. FE-SEM images of MC3T3-E1 cell cultured on the RF-sputtered Zn coating on PEO-treated Ti-6Al-4V alloy for 24 h:
(a) Ti-6Al-4V, (b) Ca/P, (c) 1 min/Zn, (d) 3 min/Zn,
(a-1) × 5,000 of (a), (b-1) × 5,000 of (b), (c-1) × 5,000 of (c), (d-1) × 5,000 of (d), (a-2) × 10,000 of (a), (b-2) × 10,000 of (b), (c-2) × 10,000 of (c), (d-2) × 10,000 of (d), (a-3) × 30,000 of (a), (b-3) × 30,000 of (b), (c-3) × 30,000 of (c), and (d-3) × 30,000 of (d).

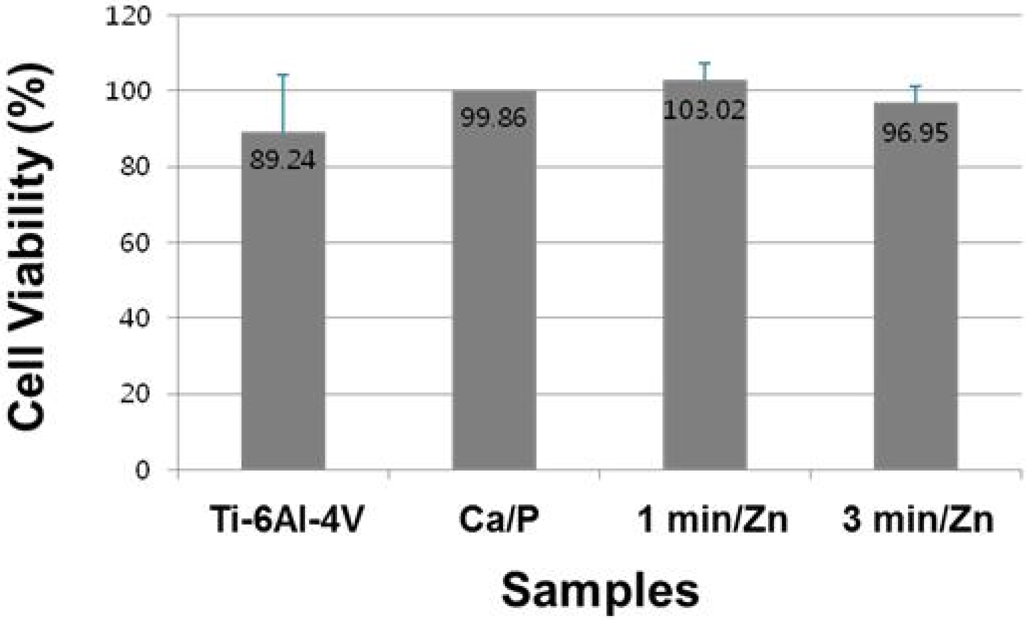

Fig. 16. The results of MTT assay for MC3T3-E1 seed on different surface conditions.

Ⅴ. CONCLUSIONS

In this study, surface characteristics of zinc coatings on the PEO-treated Ti-6Al-4V by RF-sputtering have been researched.

The results were as follows;

1. The surface of oxide films by typical of samples after PEO coating showed formation of many micro-pores with uniform distributions.

2. All the morphologies of RF-sputtered surface showed the small particles covered with droplet shapes on the pore inside and surface parts.

3. As sputtering time increased, the circular particles of Zn coatings on Ti-6Al-4V alloy increased at pore inside and surface parts.

4. As the sputtering time increased, [Ca+Zn]/P ratio for the Zn coating on the PEO-treated Ti-6Al-4V alloys increased.

5. As the sputtering time increased, the amorphous phase was increased, whereas crystal phase was decreased.

6. As a results of MTT analysis using MC3T3-E1 cell, Zn coated surface showed a higher cell proliferation rate than PEO-treated Ti-6Al-4V alloy.

- Reference -

1. D Krupa, J Baszkiewicz, JA Kozibowski, Barcz A, JW Sobzak, A Biliniski, MD Lewandowska-Szumiel, B Rajchel, Effect of calcium-ion implantation on the corrosion resistance and biocompatibility of titanium. *Biomaterials* 22 (2001) 2139.
2. XY Liu, KC Paul, CX Ding, Surface modification of titanium, titanium alloys, and related materials for biomedical applications, *Mater. Sci. Eng. R* 47 (2004) 49.
3. CG Moran, TC Horton . Total knee replacement: the Joint of the decade. *B.M.J.* 320 (2000) 820.
4. J. I. Kang, M. K. Son, H. C. Choe, W. A. Brantly, Bone-like apatite formation on manganese-hydroxyapatite coating formed on Ti-6Al-4V alloy by plasma electrolytic oxidation, *Thin Solid Films* 620 (2016) 126.
5. M. Mizuhata, Y. Mineyama, H. Maki, Fabrication of ZnS/porous silicon composite and its enhancement of photoluminesecence, *Electrochimica Acta.* 201 (2016) 86.
6. R. Palanivelu, S. Kalainathan, A. R. Kumar, Characterization studies on plasma sprayed (AT/HA) bi-layered nano ceramics coating on biomedical commercially pure titanium dental implant, *Ceramics International* 40 (2014) 7745.
7. Y. H. Jeong, H. C. Choe, W. A. Brantley, Electrochemical and surface behavior of hydroxyapatite/Ti film on nanotubular Ti-35Nb-xZr alloys, *Appl. Surf. Sci.* 258 (2012) 2129.
8. H. Wang, F. Liu, Y. Zhang, F. Wang, Structure, Corrosion resistance and apatite-forming ability of NiTi alloy treated by micro-arc oxidation in concentrated H_2SO_4. *Surf. Coat. Technol.* 206 (2012) 4054.
9. C. X. Wang, M. Wang, X. Zhou, Nucleation and growth of apatite on chemically treated titanium alloy: an electrochemical impedance spectroscopy study, *Biomaterials* 24 (2003) 3069.
10. C. Vasilescu, P. Drob, E. vasilescu, I. Demtrescu, D. Ionita, M.

Prodana, S. I. Drob, Characterisation and corrosion resistance of the electrodeposited hydroxyapatite and bovine serum albumin/hydroxyapatite films on Ti-6Al-4V-1Zr alloy surface, *Corrosion Science* 53 (2011) 992.
11. A. Bigi, M. Fini, B. Bracci, E. Boanini, P. Torrocelli, G. Giavaresi, N. N. Aldini, A. Facchini, F. Sbaiz, R. Giardino, The reponse of bone to nanocryatalline hydroxyapatite-coated Ti13Nb11Zr alloy in an animal model, *Biomaterials* 29 (2008) 1730.
12. I. J. Hwang, H. C. Choe, W. A. Brantley, Electrochemical characteristics of Ti-6Al-4V after plasma electrolytic oxidation in solution containing Ca, P, and Zn ions, *Surf. Coat. Technol.* 320 (2017) 458.
13. I. J. Hwang, H. C. Choe, Hydroxyapatite coating containing Zn and Si on Ti-6Al-4V alloy by plasma electrolytic oxidation, *Appl. Surf. Sci.* 432 (2018) 337.
14. K. V. Dijk, H. G. Schaeken, J. G. C. Wolke, J. A. Jansen, Influence of annealing temperature on RF magnetron sputtered calcium phosphate coatings, *Biomaterials* 17 (1996) 405.
15. I. S. Byeon, I. J. Hwang, H. C. Choe, W. A. Brantley, Electrochemically-coated hydroxyapatite films on nanotubular Ti-Nb alloys prepared in solutions containing Ca, P, and Zn ions, *Thin Solid Films* 620 (2016) 132.
16. S. Stojadinovic, N. Tadic, R.Vasilic, Formation and chcaraterization of ZnO films on zinc substrate by plasma electrolytic oxidation, *Surf. Coat. Technol.* 307 (2016) 650.
17. J. Katouno, K. Fujioka, S. Kidera, Y. Mabuchi, K. Sato, Y. Manome, M. Hiratsuka, H. Nakamori, H. Masuda, H. Homda, K. Hirakuri, Evaluation of the enhancement of osteogenesis by Zn-releasing dimond-like carbon film, *Diam. Relat. Mater.* 77 (2017) 131.
18. M. Long, H. J. Rack, Titanium alloys in total joint replacement-a materials science perspective, *Biomaterials* 19 (1998) 1621.
19. B. D. Ratner, A. S. Hoffman, F. J. Sheon, J. E. Lemons, Biomaterials

Science: an introduction to materials in medicine, *Elsevier Academic Press, San Diego, CA, ed.* 2 (2004) 556.
20. M. Long, H. J. Rack, Titanium alloys in the total joint replacement-a materials science perspective, *Biomaterials* 19 (1998) 1621.
21. Y. Okazaki, Y. Ito, A. Ito, T. Tateishi, Effect of alloying elements on mechanical properties of titanium alloys for medical implants, *J. inst. Metals.* 34 (1993) 1217.
22. D. R. Sumner, T. M. Turner, R. Iogloria, R. M. Urban, J. O. Galante, Functional adaptation and ingrowth of bone vary as a function of hip implant stiffness, *J. Biomechanics.* 31 (1998) 909.
23.M. McCrachen, Dental implant materials: commerially pure titanium and titanium alloys, *J. Prosthod.* 8 (1999) 40.
24. M. J. Donachie. Titanium and Titanium Alloys Source Book, *ASM, Metals Park*, *Ohio.* (1982) 3.
25. C. Chenglin, Z. Jingchuan, Y. Zhongda, L. Pinghua. Optimal design and fabrication of hydroxyapatite-Ti asymmetrical functionally graded biomaterial. *Mater Sci Eng A* 348 (2003) 244.
26. A. Ducato, L. Fratini, M. L. Casia, G. Mazzola, An Automated Visual Inspection System for the Classification of the Phases of Ti-6Al-4V Titanium Alloy, *15th International Conference CAIP2013 Part II, LNCS* 8048 (2013) 362.
27. R. Boyer, G. Welsch, E. W. Collings, Materials properties handbook: titantium alloys, *ASM, Metals Park, Ohio.* (1993) 483.
28. J. C. M. Li, Microstructure and properties of materials. 2 (1999) 12.
29. C. Sittig, M. Textor, N. D. Spencer, M. Wieland, P. H. Vallotion, Surface characterization, *J. Mater. Sci; Mater. Med.* 10 (1999) 35.
30. M. F. Hsieh, L. H. Perng, T. S. Chin, Hydroxyapatite coating on Ti-6Al-4V alloy using a sol-gel derived precusor, *Mater. Chem. Phy.* 74 (2002) 245.
31. S. H. Jeong, Y. J. Park, B. S. Kim, H. J. Song, Effects of oxygen

content on bioactivity of titanium oxide films fabricated on titanium by electron beam evaporation, *J. Nanosci. Nanotechnol.* 7 (2007) 3815.

32. D. A. Hanaor, C. C. Sorrell, Review of the anatase to rutile phase trabsformation, *J. Mater. Sci.* 46 (2011) 855.

33. M. L. Chen, J. S. Bae, W. C. Oh, Photocatalytic effect for the carbon-coated TiO_2 prepared from different heat treatment temperature, *Analytical Science & Technology* 19 (2006) 460.

34. 정용수, 박영희, 장관섭, 문성모, 최진섭, 정윤미, *실용표면처리기술 시리즈 5권 양극산화, 화신문화(주)* (2014) 281.

35. X. Liu, P. K. Chu, C. Ding, Surface modification of titanium, titanium alloys, and related materials for biomedical applications, *Mater. Sci. Eng. R* 47 (2004) 49.

36. 황인조, 최한철, PEO법을 이용한 Ti-6Al-4V 합금표면에 Ca, P, 및 Zn 도핑 효과, *한국표면공학회 학술발표회 초록집 (2016)* 146.

37. S. G. Lim, I. J. Hwang, Electrochemical Characteristics of Zn and Si Ion-doped HA Films on Ti-6Al-4V by PEO Treatment, *한국표면공학회 학술발표회 초록집 (2017)* 199.

38. I. J. Hwang, H. C. Choe, Pore shape changes and apatite formation on Zn and Si ion-doped HA films of Ti-6Al-4V after plasma electrolytic oxidation treatment, *J. Nanosci. Nanotechnol.* 18 (2018) 1442.

39. X. Liu, P. K. Chu, C. Ding, Surface modification of titanium, titanium alloys, and related materials for biomedical applications, *Mater. Sci. Eng. R* 47 (2004) 49.

40. A. Hoppe, N. S. Guldal, A. R. Boccaccini, A review of the biological response to ionic dissolution products from bioactive glasses and glass-ceramics, *Biomaterials* 32 (2011) 2757.

41. L. Yang, S. Perez-Amodio, Y. F. Florence, B. D. Groot, V. Everts, CAV. Bitterswijk, P. Habibovic, The effects of inorganic additives to calcium phosphate on in vitro behavior of osteoblasts and osteoclasts, *Biomaterials* 31 (2010) 2976.

42. W. Xue, K.Dahlquist, A. Bannerjee, A. Bandyopadhyay, S. Bose, Syntesis and characterization of triclacium phosphate with Zn and Mg based dopants, *J. Mater. Sci. Mater. Med.* 19 (2008) 2669.
43. P. J. P. Espitia, J. S. R. Coimbra, R. S. Cruz, E. A. A. Mediros, Zinc oxide nanoparticles: synthesis, antimicrobial activity and food packging applications, *Food Bioprocess Technol.* 5 (2012) 1447.
44. E. I. Get'man, T. M. Savankona, A. V.Ignatov, K. G. Diodorenko, A. Y. Talykova, L. I. Ardanova, Synthesis, characterization and electrical properties of Pb (8-x) Na2Ndx (Vo4) 60 (x/2) solid solutions, *Functional Materials.* 21 (2014) 247.
45. E. Boanini, M. Gazzano, A. Bigi, Ionic substitutions in calcium phosphates synthesized at low temparature, *Acta. Biomater.* 6 (2010) 1882.
46. R. C. Zeng, Y. Hu, F. Zhang, Y. D. Huang, Z. L. Wang, S. Q. Li, E. H. Han, Corrosion resistance of cerium-doped calcium phosphate chemical conversion coating on AZ31 magnesium alloy, *Trans. Nanoferrous Matals Soc. Chain* 25 (2016) 472.
47. S. Y. Yeong, H. C. Choe, Mn-coatings on the micro-pore formed Ti-29Nb-xHf alloys by RF-magnetron sputtering for dental applications, *Appl. Surf. Sci.* 432 (2018) 278.
48. Y. Tang, H. F. Chappell, M. T. Dove, R. J. Reeder, Y. J. Lee, Zinc incorporation into hydroxyapatite, *Biomaterials* 30 (2009) 2864.
49. E. Rocca, D. Veys-Renaux, K. Guessoum, Electrochemical behavior of zinc in KOH media at high voltage: micro-arc oxidation of zinc, *Electronanal. Chem.* 754 (2015) 125.
50. C. Chu, J. Zhu, Z. Yin, P. Lin, Optimal design and fabrication of hydroxyapatite-Ti asymmetrical functionally graded biomaterial, *Mater. Sci. Eng. A* 348 (2003) 244.
51. B. R. Stromeier, D. M. Hercules, Surfaces spectroscopic characterization of the interaction between zinc ions and γ-alumina, *Journal of Catalysis* 86 (2) (1984) 266.

52. B. D. Cullity, S. R. Stock, Elements of X-ray diffraction, Pretice Hall, *New Jersey* (2001) 388.

53. S. Y. Park, C. I. Jo, H. C. Choe, W. A. Brantley, Hydroxyaoatite deposition on micropore-formed Ti-Ta-Nb alloys by plasma electrolytic oxidation for dental applications, *Surf. Coat. Technol.* 294 (2016) 15.

54. G. Jin, H. Cao, Y. Qiao, F. Meng, H. Zhu, X. Liu, Ostrogenic activity and antibacterial effect of Zinc ion implanted titanium, *Colloids and Surfaces B: Biointerfaces* 117 (2014) 158.

55. H. Hu, et al. Antibacterial activity and increased bone marrow stem cell functions of Zn-incorporated TiO_2 coatings on titanium, *Acta. Biomaterialia.* 4 (2) (2008) 441.

56.A. I. Chum, J. G. Moralez, H. Fenniri, T. J. Webster, Helical rosette nanotubes: a more effective orthopaedic implant material, *nanotechnology* 15 (2004) 234.

57. S. Horiuchi, M. Hiasa, A. Yasue, K. Sekine, K. Hamada, K. Asaoka, E. Tanaka, Fabrications of zinc-releasing biocement combining zinc calcium phosphate to calcium phosphate cement, *J. Mech. Behav. Bioed. Mater.* 29 (2014) 151.

저작물 이용 허락서

학 과	광기술공학과	학 번	20167107	과 정	석사
성 명	한글: 황 인 조 한문 : 黃 仁 照 영문 : In-Jo Hwang				
주 소					
연락처					
논문제목	한글 : RF-sputtering법으로 PEO 처리된 Ti-6Al-4V 합금 표면에서 아연코팅 피막의 표면특성 영어 : Surface Characteristics of Zinc Coatings on the PEO-treated Ti-6Al-4V by RF-sputtering				

본인이 저작한 위의 저작물에 대하여 다음과 같은 조건아래 조선대학교가 저작물을 이용할 수 있도록 허락하고 동의합니다.

\- 다 음 -

1. 저작물의 DB구축 및 인터넷을 포함한 정보통신망에의 공개를 위한 저작물의 복제, 기억장치에의 저장, 전송 등을 허락함
2. 위의 목적을 위하여 필요한 범위 내에서의 편집・형식상의 변경을 허락함. 다만, 저작물의 내용변경은 금지함.
3. 배포・전송된 저작물의 영리적 목적을 위한 복제, 저장, 전송 등은 금지함.
4. 저작물에 대한 이용기간은 5년으로 하고, 기간종료 3개월 이내에 별도의 의사 표시가 없을 경우에는 저작물의 이용기간을 계속 연장함.
5. 해당 저작물의 저작권을 타인에게 양도하거나 또는 출판을 허락을 하였을 경우에는 1개월 이내에 대학에 이를 통보함.
6. 조선대학교는 저작물의 이용허락 이후 해당 저작물로 인하여 발생하는 타인에 의한 권리 침해에 대하여 일체의 법적 책임을 지지 않음
7. 소속대학의 협정기관에 저작물의 제공 및 인터넷 등 정보통신망을 이용한 저작물의 전송・출력을 허락함.

동의여부 : 동의(O) 반대( )

2018 년 02 월 23 일

저작자: 황 인 조 (서명 또는 인)

조선대학교 총장 귀하